Available online at www.sciencedirect.com

SciVerse ScienceDirect

Ceramics International 38 (2012) 4111–4121

CERAMICS INTERNATIONAL

www.elsevier.com/locate/ceramint

Effects of B_2O_3 and P_2O_5 doping on the microstructure evolution and mechanical strength in a lithium aluminosilicate glass–ceramic material with TiO_2 and ZrO_2

Yu-Han Wu [a,*], Kuo-Chuan Hsu [b], Chih-Hao Lee [a,c]

[a] Department of Engineering and System Science, National Tsing Hua University, Hsinchu 30013, Taiwan
[b] Ta Hsiang Containers Ind. Co., Ltd., Hsin Pu, Hsinchu 30543, Taiwan
[c] National Synchrotron Radiation Research Center, Hsinchu 30013, Taiwan

Received 12 October 2011; received in revised form 26 January 2012; accepted 26 January 2012
Available online 3 February 2012

Abstract

During the devitrification process, the coordination number of Ti changes from 4 and 5 to 6; and the coordination number of Zr changes from 6 to 8 in a lithium aluminosilicate glass–ceramic material. The flexural strength of the glass–ceramics strongly depends on the composition of additives. The strength of a well-crystallized sample increases 45% by doping with B_2O_3 and decreases 56% by doping with P_2O_5. Thermal expansion mismatch and microstructure non-uniformity are the proposed mechanisms responsible for the changes in strength. The effects of doping concentration of B_2O_3 and P_2O_5 and thermal treatment conditions on the microstructure and mechanical strength of a lithium aluminosilicate glass–ceramic material with TiO_2 and ZrO_2 were studied. The local environment around Ti and Zr correlated to the secondary phase development, such as $TiZrO_4$ and $ZrSiO_4$, during the crystallization process was observed by X-ray absorption near edge structure. The electronic structure of each peak in the X-ray absorption near edge spectra was also assigned in terms of phase evolutions. The phase transformation temperature of β-quartz solid solutions to β-spodumene solid solutions is decreased for about 100 °C by adding B_2O_3 and P_2O_5.

Keywords: Lithium aluminosilicate glass–ceramic; XANES; β-Spodumene solid solutions; Flexural strength; Low thermal expansion

1. Introduction

Lithium aluminosilicate (LAS) glass–ceramic materials have gained much attention due to their near-zero or negative thermal expansion, good mechanical strength, chemical durability and biological properties. Applications of these materials in a variety of fields, such as optical, household, electronic, architectural and military, can be developed based on their unique properties. The effect of doping with glass formers, such as B_2O_3 and P_2O_5, is one of the most interesting issues in LAS glass–ceramics because the melting, sintering and annealing temperature may be lowered. In addition, the microstructure evolution of a LAS glass–ceramics, which usually follows the sequence: the phase separation, the precipitation of the precursor phase, the nucleation and crystal growth of the main phase, the main phase transformation and the formation of the secondary phases, can also be affected significantly by these dopants. It was first proposed by Sarah et al. [1] that LAS glass–ceramics can be effectively produced in bulk form by sintering fine glass powders with the addition of B_2O_3 and P_2O_5. The result was confirmed by Shyu et al. [2,3], Sung et al. [4] and Chakraborty et al. [5]. Shyu et al. [2,3] proposed that the microstructure evolution of samples with the addition of B_2O_3 obeys the general rule of phase development sequence in LAS glass–ceramics. But the glass containing P_2O_5 shows an anomalous decrease in the amount of β-spodumene solid solution (s.s.), relative to β-quartz s.s., with increasing temperatures at a lower temperature interval (about 800–900 °C). Sung et al. [4] determined a lowered activation energy (about 23%) and crystallization temperature (approximately 56 °C) with the addition of B_2O_3 by the differential thermal analysis method. Chakraborty et al. [5] stated that the addition

* Corresponding author. Tel.: +886 35715131x34276; fax: +886 35720724.
E-mail address: yuhanwu@mx.nthu.edu.tw (Y.-H. Wu).

0272-8842/$36.00
doi:10.1016/j.ceramint.2012.01.069

of B_2O_3 and P_2O_5 has a remarkable effect on the relative amount of the two main phases and biochemical durability.

However, in the previous studies, only glass–ceramic samples with a simplified composition (Li_2O–Al_2O_3–SiO_2 and B_2O_3/P_2O_5) produced by the powder sintering method were investigated [1–5]. The details of microstructure development with a commercial-like composition prepared by a popular bulk glass-forming method are not widely reported. In a commercial composition, TiO_2 and ZrO_2 are added as nucleating agents. The structural role of these agents is also interesting to be understood. In this work, the changes of local environment of TiO_2 and ZrO_2 during the devitrification process are studied by the X-ray absorption near edge structure (XANES). The experimental results show that the coordination environment of Ti and Zr changes significantly. In addition, the effect on mechanical properties due to the different doping levels of B_2O_3 and P_2O_5 is not clear so far. Since B_2O_3 and P_2O_5 dopants will cause a variety of structural changes in the final phases, the thermal expansion coefficient [3] and the mechanical strength are expected to be altered significantly in a complex composition system. In this paper, the detailed influences of doping B_2O_3 and P_2O_5 on the microstructure and mechanical properties are discussed. It is demonstrated that the flexural strength of samples changes significantly due to the different doping levels of dopants. This phenomenon is related to the microstructural change of samples with different dopants. The main objective of this study is to demonstrate the correlations among phase development, thermal expansion coefficient and mechanical strength associated with the content of B_2O_3 and P_2O_5 added in the raw bath of a LAS glass–ceramic sample with a commercial-like recipe using a more popular monolith glass forming method [6,7].

2. Experimental procedure

2.1. Sample preparation and mechanical property measurement

Three series of LAS glass ceramic samples were prepared with nominal oxide compositions of initial charges listed in Table 1. Series A samples contain no B_2O_3 and P_2O_5 additives. Series B samples are doped with B_2O_3 and Series P with P_2O_5. The LAS glass–ceramic samples were prepared by the monolithic method [6,7]. Well-mixed industrial or analytical grade raw materials in the form of oxides and carbonates were melted in Pt or alumina crucibles at 1650–1700 °C for 2–4 h. The melting temperature and time depend on the compositions. The high temperature glass melts were poured into a metal mold and cooled to ambient temperature. The quantity of samples synthesized per batch was ~50 g for microstructure analysis or ~300 g mainly for bending test. Then the as-quenched bulk glass samples were heat treated in an electrical furnace. The degree of crystallinity is usually higher for samples with a batch of larger amount. Three thermal treatment schemes were adopted in this work. In the first scheme (scheme I), samples were heated from ambient temperature to 750 °C and held for 1 h. In the scheme II, samples were heated to 880 °C and held for 1 h. In the scheme III, samples were first heated to 880 °C; and held for 1 h, then to 1150 °C and held for another 1 h. The heating rate was ~10–12 °C/min. After heating, the samples were cooled in the furnace. The error of temperature is ±10 °C. The 750 °C and 880 °C were chosen based on the results of the literature [6,7] and our thermal mechanical analysis (TMA) data of the as-quenched samples. The relatively high heating temperature in the second step of scheme III is to clearly show the effect of secondary phases (see Section 3.2). The differences in compositions from the intial charges of heat-treated samples were verified by X-ray fluorescence and EDX. Small amount of alkaline elements (Li, Na) volatilizing are observed as expected. Glass–ceramic samples were then sliced for thermal expansion coefficient and mechanical strength measurements. Thermal expansion coefficients were measured by a TMA instrument under a heating rate of 10 °C/min in N_2 atmosphere. The mechanical strength of samples was tested by a standard three-point bending machine. Five samples were tested and averaged on each condition.

Table 1
Nominal oxide compositions (wt%).

Sample	SiO_2	Al_2O_3	Li_2O	TiO_2	ZrO_2	B_2O_3	P_2O_5	Others[a]
A01	64.2	20.1	5.0	4.1	2.0			4.6
A02	68.6	17.6	2.5	4.5	2.0			4.8
A12	65.8	20.4	5.0	2.2	2.0			4.6
A17	66.3	22.0	4.5	2.0	2.6			2.5
B01	61.2	19.1	4.7	2.0	1.8	6.9		4.3
B02	62.7	19.4	4.8	2.1	1.9	4.7		4.4
B03	64.2	19.9	4.9	2.1	1.9	2.5		4.5
B04	65.4	20.4	5.0	2.2	1.9	0.6		4.5
P10	63.0	19.6	4.8	2.1	1.9		4.1	4.5
P11	64.8	20.1	4.9	2.2	2.0		1.4	4.6
P12	65.5	20.3	5.0	2.2	2.0		0.4	4.6
P15	63.8	21.3	4.4	1.9	2.4		3.8	2.4
P16	65.7	22.0	4.5	1.9	2.4		1.1	2.4

[a] Including alkaline oxide, alkaline earth oxide, ZnO and Sb_2O_3; the contents of these components are nearly identical in all samples except sample A02, A17, P15 and P16. In most samples, ~0.6% NaO, ~1% BaO, ~1% ZnO, ~1% Sb_2O_3 and ~0.5% MgO were added but in A17, P15 and P16 only 0.3% K_2O, ~0.5% Na_2O, ~1% Sb_2O_3 and ~0.5% MgO were added.

2.2. Sample characterization

X-ray powder diffraction (XRD), XANES and scanning electron microscopy (SEM) were used to characterize the microstructure of the sample. Owing to the small amount of newly formed phase, an intense X-ray source at wiggler beamlines, BL-17A, BL-17B1 and BL-01C2 of National Synchrotron Radiation Research Center (NSRRC) was employed. An X-ray area detector, Mar 3450 image plate (IP), was used to collect the pictures of diffraction rings. By examining the intensity uniformity of the diffraction ring, the non-uniform orientation distribution and the particular large size of the microcrystallines can be identified. XRD patterns were obtained by integrating the specific arc of the diffraction rings. XANES is an element specific tool [8] and was used here to show the structural changes around Ti and Zr ions during crystallization. The Si (1 1 1) double-crystal monochromator

and Lytle detector for XANES measurement at BL-17C, BL-01C1SWLS and BL-16A were employed. The energy resolution for Ti spectra is ~0.3 eV and for Zr spectra is ~0.8 eV. Field-emission SEM (Hitachi S-4200 and LEO 1530 FEG-SEM+EDX) was used to study the morphology of crystallized samples.

3. Results and discussion

3.1. Composition and devitrification

The transparency and color of LAS glass–ceramic samples are varied by different thermal treatment conditions and compositions. Samples doped with high amount of B_2O_3 become opaque at lower heating temperatures. This result implies that the phase separation and crystallization behavior are changed by the additives. The as-quenched glass samples are transparent and yellowish because of the existence of Ti ions and trace amount of transition elements in the raw materials. After being heated at 750 °C for 1 h (scheme I), samples of series A and P still remain transparent except that the sample A01 (denoted as A01-I, where -I represents the heat treatment scheme I) and A02-I become a little darker in color than the as-quenched samples. This phenomenon might be due to the growth of separated glassy phases [9] or the change of local environments and oxidation states of the transition elements. On the contrary, series B samples become devitrified with different degrees depending on the amount of the B_2O_3 dopant. For instance, sample B02-I with 4.7% B_2O_3 is more opaque than sample B04-I containing 0.6% B_2O_3. The XRD data also show that more peaks with higher intensities appeared in sample B02-I than those in sample B04-I (see Fig. 1). This result reveals a difference in the crystallinity of these two samples. SEM micrographs (Fig. 2) also show that the grain size of sample B02-III is several times larger than that of sample B04-III, which implies the different crystal growth rates between these two samples. According to the above two results,

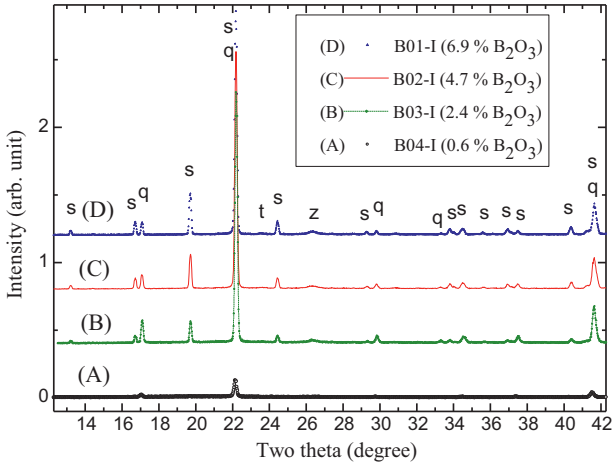

Fig. 1. XRD patterns of samples containing different proportions of B_2O_3 from 0.6% (bottom) to 6.9% (top), respectively. λ (wavelength) = 1.33295 Å. All samples are heat-treated under 750 °C for 1 h. The peaks are labeled with s: β-spodumene solid solution; q: β-quartz solid solution; z: ZrTiO4; t: TiO_2.

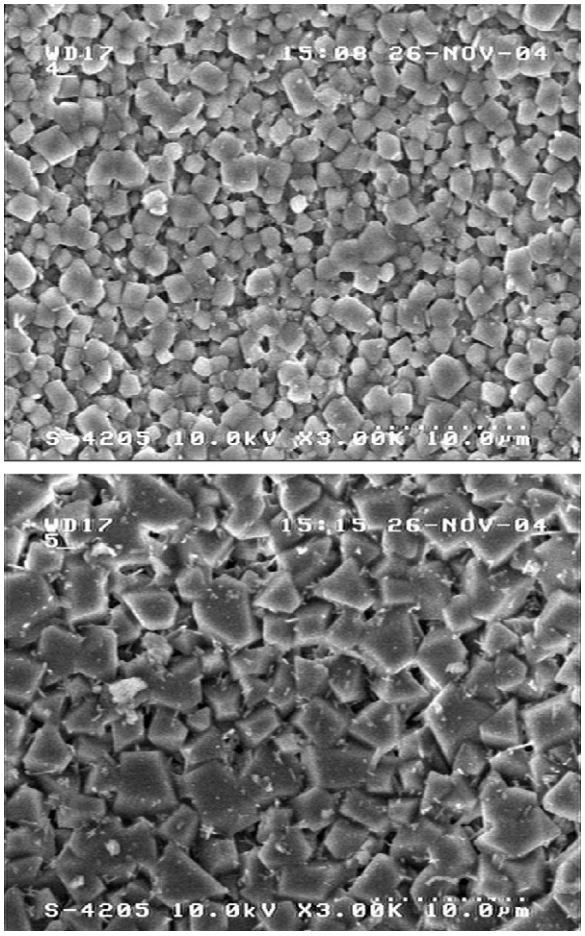

Fig. 2. SEM micrograph in a gas hole of sample B04-III and B02-III containing 0.6% (top) and 4.7% B_2O_3 (bottom), respectively. All samples are heat-treated under scheme III (1150 °C, 1 h).

samples containing more B_2O_3 are usually easier to be crystallized, as the addition of boron usually can effectively reduce the viscosity in high temperatures, enhance the mobility of ions [4] and promote the glassy phase separation [10]. In a LAS system, phase separation is usually helpful for the crystallization. Samples doped with P_2O_5 also exhibit similar phenomenon but the effect is not as strong as those samples doped with B_2O_3.

In the case of heating scheme II (880 °C, 1 h), all samples have been devitrified. Samples subjected to the heat treatment at 1150 °C for 1 h (scheme III) or a longer time with or without being held at lower temperatures are all opaque and white. The details of phase evolution are discussed below.

3.2. Microstructure development

Although the chemical constituents are complicated, phase compositions of samples can be clearly resolved by synchrotron XRD. It can be observed that the main phase transformation temperature is usually lowered when the doping concentration is increased. The vitreous state of an as-quenched glass is also verified by XRD. At heating stage, the XRD result of the series A samples (Fig. 3) suggests that the development of the main

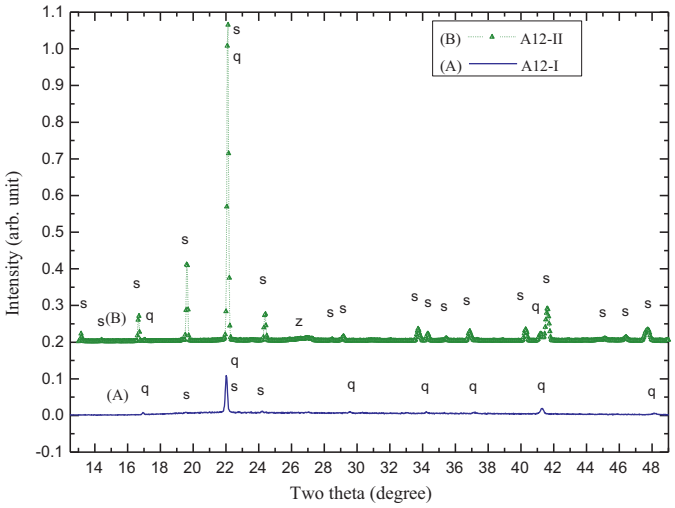

Fig. 3. XRD patterns of sample A12 (without B_2O_3 and P_2O_5) heat-treated under scheme II (top) and I (bottom). λ = 1.33295 Å; s: β-spodumene s.s.; q: β-quartz s.s.; z: $ZrTiO_4$.

phase follows a regular way, *i.e.*, hexagonal β-quartz solid solution (s.s.) forms at a lower temperature (about 750 °C for 1 h) and transforms to tetragonal β-spodumene s.s. at a higher temperature (about 880 °C for 1 h). Fig. 1 is an example showing that the transformation temperature of β-quartz s.s. to β-spodumene s.s. is decreased when B_2O_3 is added in the raw batch. Indeed from the XRD data of samples containing 6.9–0.6% B_2O_3, it can be found that higher content of B_2O_3 results in a formation of larger amount of β-spodumene s.s. under the same thermal condition (scheme I). Similar effects can also be observed in samples doped with P_2O_5. For example, the XRD pattern of sample P15-II (3.8% P_2O_5) shows clear peaks of β-spodumene s.s. but these peaks are almost invisible in the XRD pattern of sample P16-II (1.1% P_2O_5) shown in Fig. 4. Moreover, no clear diffraction peaks was observed in sample A17-II while peaks belong to β-spodumene s.s. can be identified in sample heated at a higher temperature (A17-III). Here A17 (without doping of P_2O_5) is the reference sample with the same ratio of basal composition of P-15 and P-16 (Table 1). Therefore, the phase transformation temperature is decreased due to the addition of P_2O_5. For comparison, a simplified composition, Li_2O–Al_2O_3–SiO_2 batch, with only P_2O_5 being added was prepared under the same condition. The manner of phase evolution by XRD patterns still exhibits nearly identical result. This phenomenon of lowering phase transformation temperature is roughly consistent with the work of Chakraborty et al. [5]. It might be due to the weakening effect of silicate network by these additives. Some strong Si–O bonds are replaced by B–O or P–O bonds. The distorted bonding and charge compensated ions might destroy the glass network. Consequently, the lower viscosity and higher diffusion rate in a glass matrix can benefit the transformation of β-quartz s.s. to β-spodumene s.s. However, in accordance with the report of Shyu et al. [2,3], the quantity of β-spodumene s.s. varied with the content of P_2O_5 in a non-linear fashion and an anomalous drop was found with an increasing temperature between 800 and 900 °C. This inconsistent result might be due to the different synthetic process and composition.

The peak position of high-temperature phase (β-spodumene s.s.) shifts with heating temperatures. After being heated under scheme III (1150 °C, 1 h), the β-spodumene s.s. as the major phase has been identified in all samples by the XRD method (see Fig. 5 as an example). By comparing with patterns of lithium aluminosilicates in ICDD database, such as $Li_{0.6}Al_{0.6}Si_{2.4}O_6$ (JCPDS file no. 21-0503), $Li_2O.Al_2O_3.4SiO_2$ (JCPDS file nos. 74-1106, 35-0797, 71-2058) and $Li_2O{\cdot}Al_2O_3{\cdot}6SiO_2$ (JCPDS file no. 35-0794), it can be found that the samples subjected to a higher heat-treatment temperature often exhibit higher values of d-spacing of β-spodumene s.s. as listed in Table 2. For example, the d-spacing of β-spodumene s.s. of sample B02-I, nearly identical to the d-spacing data shown in JCPDS no. 21-0503, is smaller than that of B02-II and B02-III

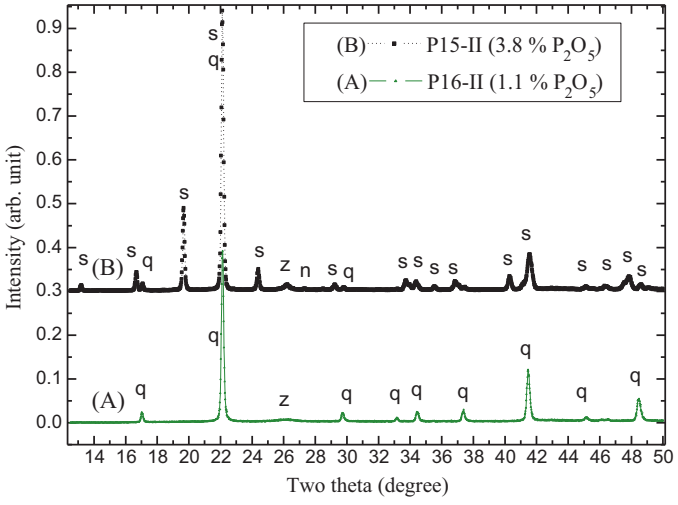

Fig. 4. XRD patterns of samples containing 3.8% (bottom) and 1.1% (top) P_2O_5, respectively. All the samples are heat-treated under 880 °C for 1 h (scheme II). λ = 1.33295 Å. s: β-spodumene s.s.; q: β-quartz s.s.; z: $ZrTiO_4$; n: Zn_2SiO_4.

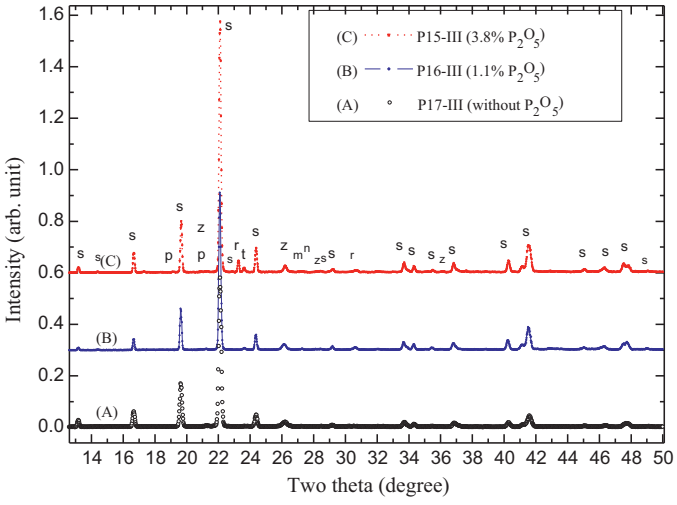

Fig. 5. XRD patterns of samples containing different proportions of P_2O_5. All the samples are heat-treated under scheme III (1150 °C, 1 h). λ = 1.33295 Å; s: β-spodumene s.s.; z: $ZrTiO_4$; n: Zn_2SiO_4; r: $ZrSiO_4$, m: $MgSiO_3$.

Table 2
Comparison of d-spacing (Å) of β-spodumene solid solutions.

Sample	(1 0 1)	(1 1 1)	(1 0 2)	(2 0 1)	(2 1 1)
B02-I	5.775	4.572	3.882	3.456	3.143
B02-II	5.807	4.589	3.900	3.471	3.154
B02-III	5.807	4.589	3.900	3.474	3.154
P15-II	5.799	4.595	3.900	3.474	3.154
P15-III	5.807	4.600	3.904	3.477	3.159
P16-III		4.595	3.916	3.480	3.159
JCPDS 35-0797		4.6087	3.9134	3.4865	3.1641
JCPDS 35-0794		4.5827	3.8848	3.4674	3.1483
JCPDS 21-0503		4.572	3.870	3.462	3.1431

The error bar in our data: ±0.005 Å.

by about 0.02 Å. While the d-spacing of the latter two is almost the same, this implies that the crystal structure in this parent glass is quite stable when the heating temperature is higher than 880 °C. The phenomenon of variation in d-spacing can also be observed in the samples containing P_2O_5. The values of d-spacing of this experiment are usually located between the values of $Li_2O{\cdot}Al_2O_3{\cdot}4SiO_2$ and $Li_2O{\cdot}Al_2O_3{\cdot}6SiO_2$ in JCPDS files. The slight shift of peak positions may be due to the difference in chemical composition or residual stresses.

Moreover, some peaks of minor phases, presumed to be $ZrTiO_4$, rutile TiO_2 and spinel of zinc and magnesium, are also identified in the samples subjected to heating scheme III. Because of the very small grain size and amount, the diffraction peaks of these secondary phases are often very weak and broad. Only some main peaks of the above phases can be recognized. The result of the existence of minor phases is consistent with XANES data of this work and the study of other groups [11–14]. The peak intensities of the minor phases are usually very small or cannot be seen when the sample is only heated at lower temperatures. This result indicates that a higher temperature process usually benefits the development of these minor phases. The reason for the above phenomena may be due to the different solubility between β-quartz s.s. and β-spodumene s.s. [6,7]. When the main phase transformation occurs, the solubility of impurity ions in β-spodumene s.s. exceeds the solubility limit and the ions are excluded from the main phase. Besides, higher temperatures are helpful in the migration of those ions.

The morphology change of the secondary phases is also interesting. The SEM micrograph of sample A02-III with 4.5% TiO_2 was shown in Fig. 6. It demonstrates that the needle-like Ti and Zr-rich (determined by EDX) secondary phases, presumed as $ZrTiO_4$, precipitated at the grain boundaries of the main phase. $ZrTiO_4$ can also be observed at the grain boundaries in the samples of A01-III, A12-III and B04-III. The XRD and SEM results show that $ZrTiO_4$ usually appears when the samples are heated at 1150 °C. This temperature range is consistent with a previous study showing that $ZrTiO_4$ solid solution is thermodynamically stable above 1100 °C [15]. However, it seems that some Ti and Zr-rich crystallites may agglomerate inside β-spodumene s.s. grains (white spots in the SEM image) and a precipitation free zone near grain boundaries may be observed. In addition, there are more Ti and Zr-rich

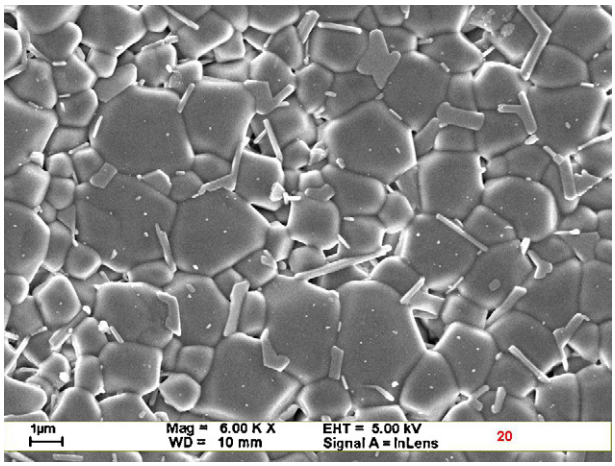

Fig. 6. SEM micrograph of sample A02-III containing 4.5 wt% TiO_2 (electron backscattering mode). The sample is heated-treated under scheme III (1150 °C, 1 h).

crystallites in large main-phase grains than in small main-phase grains. This might be due to the longer diffusion distance to the grain boundary. Consequently, these crystallites tend to coalesce inside a grain to reduce the free energy. When the TiO_2 concentration is lowered, the number of white spots inside a grain is decreased. It is interesting to note that a change of composition ratio of TiO_2 to ZrO_2 results in different amounts of rutile TiO_2 and $ZrTiO_4$ precipitates, which can be determined by the XRD peak intensities. For instance, sample A01-III with 4.0% TiO_2 shows a few peaks of rutile TiO_2 and $ZrTiO_4$, while only the diffraction peaks of $ZrTiO_4$ can be identified in sample A12-III with only 2.2% of TiO_2 at the initial charge.

3.3. XANES spectral features

To further understand the effects of TiO_2 and ZrO_2 as nucleating agents, the XANES studies of titanium and zirconium K-edges for LAS glasses and glass–ceramics are briefly reported here. A significant change of XANES spectra of Ti and Zr edges under different thermal schemes was found

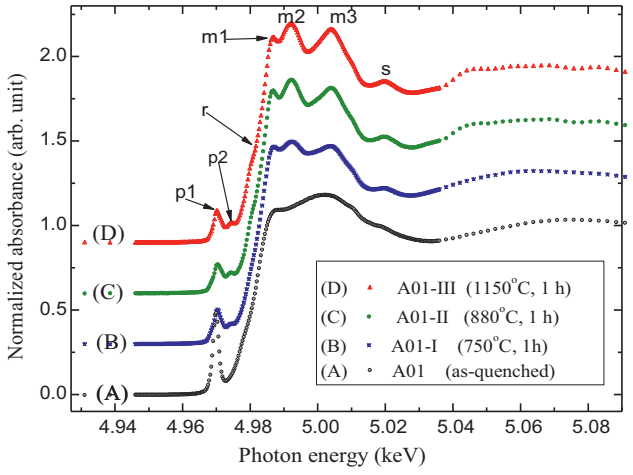

Fig. 7. XANES spectra of Ti K-edge of sample A01 under different heat treatment conditions (shifted for clarity).

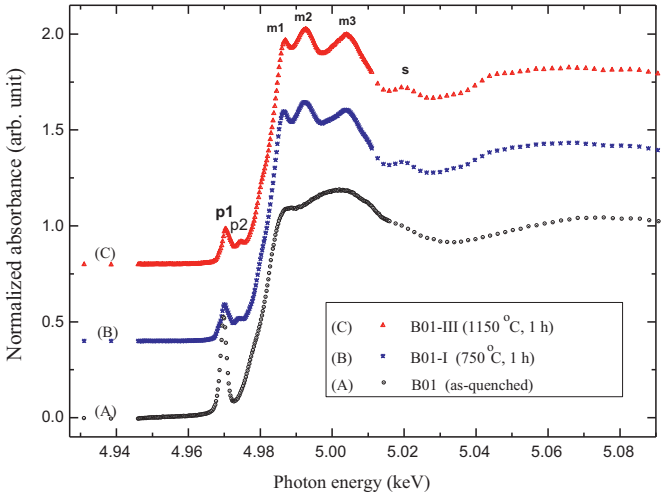

Fig. 8. XANES spectra of Ti K-edge of sample B01 under different heat treatment conditions (shifted for clarity).

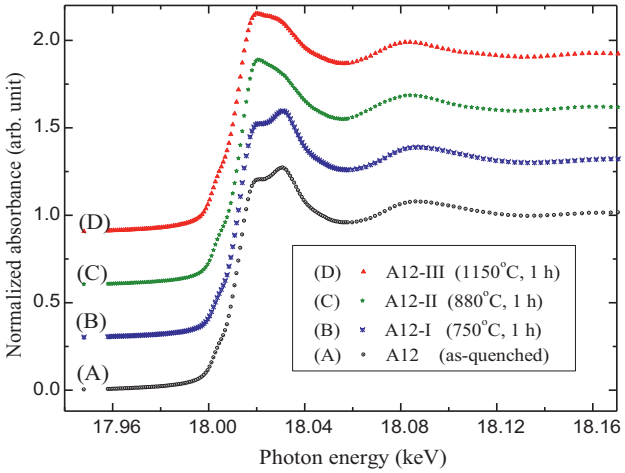

Fig. 10. XANES spectra of Zr K-edge of sample A12 under different heat treatment conditions (shifted for clarity). The spectra of samples doped with P_2O_5 in this study are similar to this figure.

(as shown in Figs. 7–11) in the present compositions. This result confirms that these two elements are usually involved in the crystallization process when more than 2 wt% of TiO_2 and ZrO_2 are added. Typical XANES spectra at Ti K-edge of a sample containing 4 wt% TiO_2 (A01) under different thermal schemes are shown in Fig. 7. Two pre-edge peaks (denoted as "p1" and "p2"), a shoulder (denoted as "r") in the edge jump and three main edge crests ("m1", "m2" and "m3") can be recognized. However, only part of the above features (p1, m1 and m3) can be identified in the vitreous samples. For rutile TiO_2, usually another minor pre-edge peak before p1 can be found [16–22]. However, no discernible pre-edge peak before p1 can be resolved in our spectra. This peak might be buried by the stronger p1 peak in our samples or it is masked due to the Zr contribution. Although great efforts on theoretical and experimental works have been carried out on XANES of Ti and other *3d* transition elements [16–29], there is very few report talking about the XANES peak assignments of these elements related to the phase evolution in LAS glass–ceramic materials [30,31]. Further discussions of the peak assignment and its origins are briefly mentioned below.

3.3.1. The intensities and energy positions of the Ti pre-edge peaks

The variation of pre-edge peak intensities and positions is a sign of local environment change, and the information of symmetry site and coordination number of the element studied can be obtained. The pre-edge peak p1 corresponds to a partially allowed *1s* to *3d* core level dipolar transition with *p–d* mixing [16,17,19,24,28,31]. Table 3 summarizes normalized intensities of pre-edge peaks (p1) of the samples. It can be found that the intensity usually drops down more than ~50% and approaches a constant (~0.2–0.3) gradually when the sample transforms from an amorphous one to a highly crystalline solid. The pre-edge peak intensity is proportional to the percentage of the unoccupied *p* density of states in the *p–d* hybridization. The bond angle variance and site distortion from disorder will give rise to an increased *3d–4p* orbital

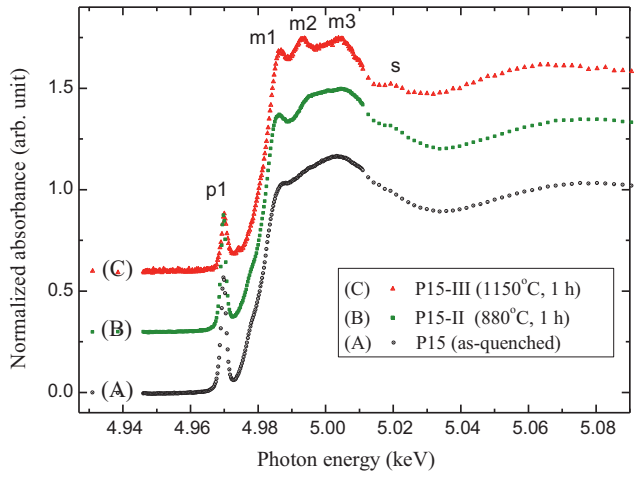

Fig. 9. XANES spectra of Ti K-edge of sample P15 under different heat treatment conditions (shifted for clarity).

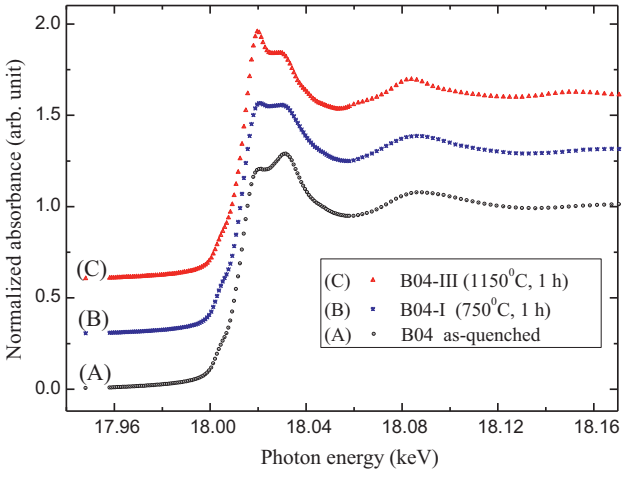

Fig. 11. XANES spectra of Zr K-edge of sample B04 under different heat treatment conditions (shifted for clarity). The spectra of samples doped with different amount of B_2O_3 in this study are nearly identical.

Table 3
Data of pre-edge peak p1 of Ti K-edge.

Sample	Pre-peak data	
	Position (eV)	Normalized height
A01	4970.0	0.48
A01-I	4970.3	0.20
A01-II	4970.3	0.17
A01-III	4970.0	0.19
A12	4969.8	0.55
A12-I	4969.8	0.53
A12-II	4969.8	0.27
A12-III	4969.8	0.28
B01	4969.8	0.52
B01-I	4970.0	0.19
B01-III	4970.3	0.19
B02	4969.8	0.53
B02-I	4970.0	0.22
B02-III	4970.0	0.21
B04	4969.8	0.56
B04-I	4969.8	0.34
B04-III	4970.0	0.24
A17	4968.8	0.58
A17-II	4969.8	0.43
A17-III	4970.0	0.32
P15	4969.8	0.57
P15-II	4969.8	0.54
P15-III	4970.0	0.28
P16	4970.0	0.60
P16-I	4970.0	0.51
P16-II	4970.0	0.47
P16-III	4970.0	0.33

hybridization. The *1s* to *nd* transitions are not allowed for a complete centrosymmetric site (*e.g.*, octahedral site) due to the selection rule. As a result, the higher intensity of pre-edge peaks of vitreous samples indicates that most of the Ti atoms are in a non-centrosymmetric environment (*e.g.*, tetrahedral or distorted octahedral site) of the glassy samples. After devitrification, the lowered intensity of pre-edge peaks implies that Ti atoms have been incorporated into an ordered structure (*e.g.*, crystalline phase). More precisely, the coordination number of Ti can be obtained by using both the pre-edge peak intensity and the energy position of the peak because these data are directly correlated to the degree of *p–d* mixing, site distortion and oxidization states. By comparing our XRD and XANES data with the literature [20,25,29,31], it can be roughly estimated that the coordination number of Ti is ~40% fourfold (TiO_4, Ti as a network former) combined with ~60% fivefold (TiO_5) in most of our glassy samples and ~10% fourfold combined with ~90% sixfold (TiO_6) in the highly crystalline samples (scheme III). This result for the vitreous samples is roughly consistent with the previous studies related to Ti-bearing glasses [31–35]. A sample with a composition containing more B_2O_3 (such as sample B01-III) or more Ti doped (such as sample A01-III) usually has a lower pre-edge peak intensity. This result indicates that more sixfold Ti bonds are formed during the devitrification process.

A second feature of the pre-edge peak was denoted as ''p2'' which can be well-resolved in samples B01-III and A01-III (Figs. 7 and 8). The split pre-edge features are usually ascribed to the quadrupole and dipole transitions to the *3d*/*4p* molecular bands split by the crystal field [28]. The two lowest unoccupied rutile TiO_2 molecular bands are divided into two groups: the threefold t_{2g} and the twofold e_g. These bands are also splitted due to the slight distortion of TiO_6 octahedron. The p1 and p2 peaks were assigned as t_{2g} and e_g-like final states due to dipolar transitions from Ti *1s* orbit [18,23]. In our experiments, the p2 peaks can be clearly identified in the samples doped with B_2O_3 or with higher content of TiO_2 after scheme III heat treatment. It indicates that a medium-range ordering of molecular orbits of rutile TiO_2 was formed. However, near edge peaks should also be taken into consideration when the medium-range environment around the photoabsorber is concerned. We will describe near edge peaks in the following.

3.3.2. Near edge peaks of Ti

In near edge structures, the feature change also reveals an electronic structure change and microstructure change around the element studied. The sharp jump of the main absorption K-edge is due to the ionization of the *1s* core electron by X-ray photons with energy higher than the characteristic binding energy of *1s* orbit. The first peak of the main feature denoted as ''m1'' (see Figs. 7–9) might be due to the multiple scattering contribution from the presence of next nearest neighbors, such as O or Ti, around Ti [25] or *1s* to *4p* transition. The second and third peaks (m2 and m3) are attributed to the electron transitions from *1s* to the *4p* and higher-lying *p*-states [19,21]. In the present work, the main absorption features can be well-resolved in a highly crystalline sample while only smooth and broadened shoulders of m1 and m3 can be observed in a vitreous sample. These results are consistent with the expected medium-range environment of Ti atoms in a crystalline structure after devitrification mentioned in the preceding paragraph. In an amorphous system, the main features mainly come from the first shell and the contribution from outer shells submerges due to the lack of a long range order. The statistical variation in the edge position among various absorption sites from aperiodicity results in a broadened XANES and EXAFS (Extend X-ray Absorption Fine Structure) features. Therefore, the feature ''s'' shown in Figs. 8 and 9 denoted as the first EXAFS peak is absent in our vitreous samples. Moreover, the degree of Debye–Waller-like damping due to a random phase decoherence among each set of multiple scattering path is also another important factor for amorphous materials [25]. In addition to the disorder described above, another reason of the low main-edge peak intensity of a vitreous sample is the well-known f-sum rule [25,36]. The f-sum rule, following the Kramers–Kronig relation, infers that the entire absorption integrated over all energy ranges and absorption edges is a constant independent of the final state. Hence, aperiodic array typically broadens spectra without changing the total integrated strength. In this study, samples with different dopants exhibit different near edge features. The feature change can be adopted to understand the crystalline phase development in a sample. A sample doped with higher content of TiO_2 or B_2O_3 being easier to crystallize usually reveals more pronounced main edge features even at lower heat treatment temperatures. This result

indicates that these samples have lower energy barriers for crystallization which also agrees with the XRD results. The main absorption peaks of the P_2O_5 bearing samples after scheme II and III heat-treatment (shown in Fig. 9) are not well-resolved as those samples doped with B_2O_3 or with higher content of TiO_2. It implies that Ti ions are in a more disordered environment. The SEM and XRD results also shows that higher amount of glassy phases are present in samples with P_2O_5. Thus, the effect of P_2O_5 to benefit crystallization seems not as significant as B_2O_3 and TiO_2 for the composition studied. Furthermore, the whole feature of XANES spectra (Figs. 7–9) of samples subjected to scheme III thermal treatment is similar to the spectra of rutile TiO_2 or $ZrTiO_4$ [20,37,38] compounds. This result can be considered as indirect evidence to confirm the existence of $ZrTiO_4$ and/or rutile TiO_2 after crystallization in most of our samples. $ZrTiO_4$ and rutile TiO_2 both exhibit sixfold Ti in slightly distorted octahedral sites and this coordination environment is consistent with the information obtained from the study of pre-edge peaks. The remained fourfold Ti atoms might exist in residual glassy phases. The information from the relative intensity ratio of the three main absorption peaks, similar to the result from XRD data, also indicates that a higher content of Ti in an initial charge may result in more rutile TiO_2 formation than that of $ZrTiO_4$. Furthermore, some subtle changes around the photoabsorber can be observed by XANES rather than by XRD. For instance, the feature of XANES spectra of sample A01-I reveals a significant change after heat treatment (750 °C, 1 h). Only an amorphous halo can be observed in the XRD pattern. This situation might be due to a behavior of the ion aggregation, or micro-phase separation of the glass matrix or the formation of some Ti-rich precursor phases with very small size.

3.3.3. The absorption spectra of Zr K-edges

The spectra of Zr K-edge also present different features under varied heat treatment conditions and compositions, as demonstrated in Figs. 10 and 11. The spectra of a sample doped with P_2O_5 have similar features as those of the sample A12 (Fig. 10). Although samples with the addition of B_2O_3 exhibit different XANES spectra among samples with the other dopants (see Fig. 11), they have nearly identical spectra features insensitive to the different doping levels of B_2O_3. The different in Zr XANES features of samples with different additives might be due to the formation of different secondary phases. These spectra of samples with B_2O_3 usually begin to alternate at a lower thermal treatment temperature (scheme I) and show a zircon ($ZrSiO_4$)-like feature at a higher temperature (scheme III). This result is also consistent with the information obtained from XRD. Three main peaks of $ZrSiO_4$ can be resolved in the XRD patterns of these B_2O_3-containing samples under scheme III thermal treatment while only one or two of them with low intensity can be found in samples doped with P_2O_5. This result might be due to that some B atoms have replaced the Si atoms in the aluminosilicate network and the excessive silicates react with Zr. Since Zr ions react with silicates to form $ZrSiO_4$, there is not enough residual Zr ions remained in these samples to form $ZrTiO_4$. Thus, there will be more $ZrSiO_4$ and less $ZrTiO_4$ (more rutile TiO_2) in a B_2O_3-beating sample. From XRD data, some XRD peaks and Ti XANES features belong to rutile TiO_2 rather than $ZrTiO_4$ can be more easily found in the B_2O_3-bearing samples even at heating scheme I (750 °C). On the contrary, no rutile TiO_2 peaks can be observed for other samples without B_2O_3 under the scheme I thermal condition. For P_2O_5-bearing samples subjected to the scheme III heat treatment, there are usually 3–4 main XRD peaks of $ZrTiO_4$ which can be identified, but only the strongest $ZrTiO_4$ peak with very low intensity can be found in samples doped with B_2O_3. Therefore, the high temperature B_2O_3-bearing samples exhibit a $ZrSiO_4$-like feature while other sample systems without adding B_2O_3, although with the same amount of Ti doping, do not have the same evolution manner of secondary phase and show a different Zr XANES feature. Furthermore, by comparing with the spectra of the literature [39], the coordination number of Zr tends to increase from six to eight as the sample transformed from an amorphous matter into a highly crystalline material. Since the Zr ion in $ZrSiO_4$ is eightfold coordinated and sixfold coordinated in $ZrTiO_4$, the spectra of samples with B_2O_3 shows the most significant eightfold bonding feature due to the lack of $ZrTiO_4$. Because no evidence shows the existence of sevenfold coordinated Zr-bearing mineral, the other samples without B_2O_3 might exhibit a mix of 6-coordinated and 8-coordinated sites. The eightfold bonding feature is not so obvious due to the minor amount of $ZrSiO_4$ in samples without B_2O_3. However, the result of changes of coordination number is inconsistent with the previous work of Ramos and Gandais [31] with LAS composition but is consistent with the research result of Dumas et al. in a cordierite glass–ceramics [40]. The spectra in the study of Ramos et al. remained nearly identical at all stages of heat treatments while our results show significant differences. The cause of inconsistency is still not known at this stage.

3.4. Mechanical strength

The flexural strength of a final product (scheme III, heat-treated under 1150 °C, 1 h) strongly depends on the doping level of different additives. Fig. 12 demonstrates the measured flexural strength as functions of concentrations of B_2O_3 and P_2O_5 additives. Though the flexural strength is lower than that of most commercial products (~100 MPa), the relative value and tendency still can be discussed. The lowered strength could be attributed to the existence of gas holes and the short nucleation period of our samples. It can be observed from Fig. 12 that the mechanical strength of samples doped with B_2O_3 is usually higher than that of samples with P_2O_5. The doping of 4 wt% B_2O_3 in a sample increases the strength from 62 MPa (633 kgf/cm^2) to 90 MPa (920 kgf/cm^2) approximately; while the addition of P_2O_5 results in a significant decrease (more than 50%) in strength. Possible explanations of this tendency are illustrated below:

(1) The difference in thermal expansion coefficient among phases: The origin of internal stress of glass–ceramics usually derives from the difference of thermal expansion coefficients (CTE) of various phases. During heating or

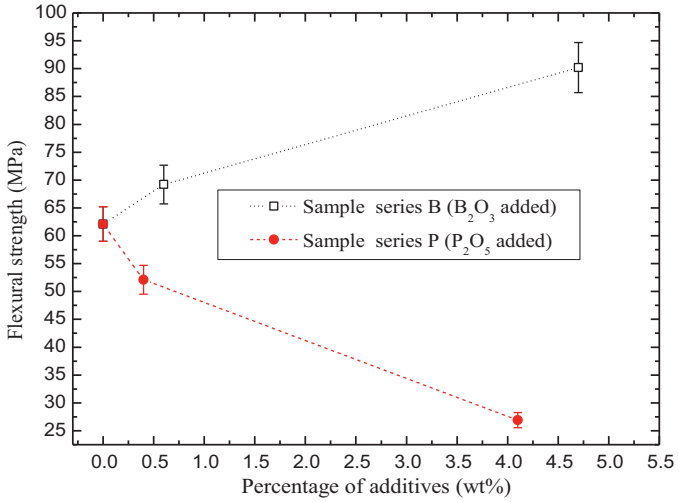

Fig. 12. The flexural strength as functions of weight percentage of B_2O_3 or P_2O_5 as additives.

cooling, huge thermal stress could be generated in composite materials between the neighboring phases with a large difference in CTE. For samples doped with P_2O_5, the negative CTE belong to the main phase and the positive CTE belong to the secondary phase may cause a large thermal expansion mismatch and thus a huge residual internal stress is formed. The result of TMA shows that the linear CTE of samples with 4.1% P_2O_5 (sample P10-III) is about -0.38×10^{-6}/°C (27–500 °C, negative value) while the CTE of samples containing 4.7% B_2O_3 (B02-III) is about 1.38×10^{-6}/°C (27–500 °C, positive value). This result indicates that a significant difference in CTE among phases of sample P10-III is formed, because, according to our knowledge, only the main phase owns negative CTE in the present phase composition system, *i.e.*, the CTE of the main phases largely depend on the phase composition and the general values are listed below: β-quartz s.s. is $\sim 0.15 \times 10^{-6}$/°C and β-spodumene s.s. is $\sim 2 \times 10^{-6}$/°C [6,7]. Since the contribution of CTE from minor phases is very small, it can be inferred that the CTE of the main phase of samples doped with B_2O_3 is positive but it is negative for samples containing P_2O_5. Consequently, samples containing B_2O_3 exhibit relatively lower CTE mismatch between phases resulting in lower internal stresses and show a higher flexural strength.

(2) Microstructure uniformity: The effect of secondary phase formation is important. From XRD and SEM results, a sample doped with P_2O_5 exhibits more different kinds of minor phases than that of adding B_2O_3. It is usually difficult to relax thermal stresses when more secondary phases appeared due to the larger differences in CTE. The effect of main crystalline phase distribution is also critical for flexural strength. According to the IP images, the diffraction rings of samples containing P_2O_5 are not continuous; instead, they form a diffraction ring decorated by diffraction spots. This result indicates that these samples are not uniform small crystalline powders. The grain size and grain distribution over the glass matrix are not uniform under present thermal treatment conditions. Thus the resistance to the crack elongation of crystalline phases is not so effective. On the contrary, the diffraction rings of the reference sample, A12-III, and a sample doped with B_2O_3 show a feature of more complete diffraction rings, similar to a perfect powder, so that the cracks may not elongate so easily in the matrix. SEM results also show that the particle size distribution of samples doped with B_2O_3 is relatively uniform compared with that of samples doped with P_2O_5. For example, some of the grains of P11-III (doped with P_2O_5) are larger than 5 μm. It is well-known that when the particle size distribution is irregular and the size of grains is larger than several μm, the strength usually drops in ceramic materials [41]. Furthermore, from SEM images, it seems that micro-cracks have been formed caused by a minor precipitate in sample P10-III. Besides, when the content of B_2O_3 is higher, more gas bubbles are refined resulting in fewer pores during melting process. The effects of micro-cracks and pores on strength are usually unfavorable.

(3) The ability of additives to relax the internal stress: It is well-known that adding B_2O_3 can drastically reduce the viscosity of a glass matrix of a sample under thermal treatment, because the softening point is lowered for several tens of degrees. As the effect of decreasing viscosity by doping P_2O_5 is usually not so significant, adding B_2O_3 may effectively relax the thermal stresses among phases by viscous flow during heating or cooling. Consequently, B_2O_3-doped samples have higher strength than P_2O_5-doped samples and the sample without doping (A12-III).

(4) The formation of Ti-rich needle-like phase: A previous work done by Lee et al. [42] showed that Ti-rich whisker phases precipitated at grain boundaries of the main phase enhanced the strength of a LAS glass–ceramic sample. Similar phase assemblage was also found in some of our samples, such as samples A01-III, A12-III and B04-III, resulting in an increase of strength. However, this kind of phase assemblage cannot be observed clearly in samples containing P_2O_5.

Therefore, the flexural strength of samples doped with P_2O_5 displays a lower strength than that of samples with B_2O_3 due to the complicated and non-uniform nature in microstructure. Nevertheless, large difference in the thermal expansion of the main phase, secondary phases and residual vitreous phases still should be responsible for this lowered strength phenomenon in some degree.

4. Conclusion

LAS glass–ceramic samples with commercial-like compositions have been prepared by the monolith glass-forming method and characterized by XRD and XANES. The general conclusions are as follows:

(1) The additives, especially B_2O_3, often result in a lower transformation temperature of β-quartz s.s. to β-spodumene s.s. This phenomenon might be due to the decrease in

viscosity of the glass matrix. In the present composition system, the phase development sequence still obeys the general way, *i.e.*, β-quartz s.s. formed at a lower temperature and transformed to β-spodumene s.s. at a higher temperature.

(2) Various secondary phases, such as $ZrTiO_4$, rutile TiO_2, and spinel of zinc and magnesium are usually precipitated at higher temperatures (1150 °C). A needle-like Ti-rich phase can be found at grain boundaries of the main phase in most of the samples without P_2O_5.

(3) The change of XANES spectra (with composition of ∼2 wt% TiO_2 and ZrO_2) confirmed that Zr and Ti are usually involved in the crystallization process and the XANES features also identify the existence of some minor phases ($ZrTiO_4$ or rutile), which usually cannot be clearly identified by XRD. The elements (Ti or Zr) studied often change from lower to higher coordination state when the sample transforms from an amorphous to a highly crystalline solid. For instance, the coordination number of Ti was changed from 4 and 5 to 6 and the coordination number of Zr changed from 6 to 8 as described by the XANES peak assignments relating to the microstructure evolution.

(4) Samples containing B_2O_3 show an increased flexural strength while samples with P_2O_5 exhibit a lowered strength. The difference of strength between dopant-free samples and samples with 4% additives can be higher than 30 MPa approximately. Possible mechanisms corresponding to microstructure and thermal expansion coefficients are proposed.

Acknowledgement

The authors would like to thank for the generous beamtime support of NSRRC in Taiwan.

References

[1] K. Sarah, R.T. Michelle, L. Samuel, Sinterable, β-Spodumene glass–ceramics, J. Am. Ceram. Soc. 72 (1989) 1873–1879.

[2] J.J. Shyu, M.T. Chiang, Sintering and phase transformation in B_2O_3/P_2O_5-doped $Li_2O{\cdot}Al_2O_3{\cdot}4SiO_2$ glass–ceramics, J. Am. Ceram. Soc. 83 (2000) 635–639.

[3] J.J. Shyu, H.H. Lee, Sintering, crystallization and properties of B_2O_3/P_2O_5-doped $Li_2O{\cdot}Al_2O_3{\cdot}4SiO_2$ glass–ceramics, J. Am. Ceram. Soc. 78 (1995) 2161–2167.

[4] Y.M. Sung, A.D. Stanley, A.K. James, The effect of boria and titania addition on the crystallization and sintering behavior of Li_2O–Al_2O_3–$4SiO_2$ glass, J. Eur. Ceram. Soc. 14 (1994) 455–462.

[5] S. Chakraborty, R.K. Chaturvedi, R. Pyare, In vitro characterisation and microstructure of B_2O_3/P_2O_5 doped bioactive spodumene glass–ceramics, Adv. Appl. Ceram. 106 (2007) 216–221.

[6] W. Holand, G.H. Beall, Glass–Ceramic Technology, The American Ceramic Society, Westerville, OH, 2002.

[7] H. Bach, K. Dieter, Low Thermal Expansion Glass Ceramics, Springer, Berlin, 1995.

[8] I. Tanaka, T. Mizoguchi, T. Yamamoto, XANES and ELNES in ceramic science, J. Am. Ceram. Soc. 88 (2005) 2013–2029.

[9] M.J. John, S.S. Marie, L.O. Renee, E.S. James, Effect of heat-treatment temperature on the properties of a lithium aluminosilicate glass, J. Am. Ceram. Soc. 74 (1991) 92–97.

[10] V. Werner, Phase separation in glass, J. Non-Cryst. Solids 25 (1977) 170–214.

[11] V. Maier, G. Müller, Mechanism of oxide nucleation in lithium aluminosilicate glass–ceramics, J. Am. Ceram. Soc. 70 (1987) C-176–C-178.

[12] G.H. Beall, Design and properties of glass–ceramics, Annu. Rev. Mater. Sci. 22 (1992) 91–119.

[13] L. Arnault, M. Gerland, A. Rivi Ere, Microstructural study of two LAS-type glass–ceramics and their parent glass, J. Mater. Sci. 35 (2000) 2331–2345.

[14] P. Riello, P. Canton, N. Comelato, S. Polizzi, M. Verita, G. Fagherazzi, H. Hofmeister, S. Hopfe, Nucleation and crystallization behavior of glass–ceramic materials in the Li_2O–Al_2O_3–SiO_2 system of interest for their transparency properties, J. Non-Cryst. Solid 288 (2001) 127–139.

[15] A.E. Mchale, R.S. Roth, Low-temperature phase relationships in the system ZrO_2–TiO_2, J. Am. Ceram. Soc. 69 (1986) 827–832.

[16] L.A. Grumes, Study of the K-edges of *3d* transition metals in pure and oxide form by X-ray absorption spectroscopy, Phys. Rev. B 27 (1983) 2111–2131.

[17] R. Brydson, H. Sauer, W. Engel, J.M. Thomas, E. Zeitler, N. Kosugi, H. Kuroda, Electron energy loss and X-ray absorption spectroscopy of rutile and anatase: a test of structural sensitivity, J. Phys. Condens. Matter 1 (1989) 797–812.

[18] B. Poumellec, P.J. Durham, G.Y. Guo, Electronic structure and X-ray absorption spectrum of rutile TiO_2, J. Phys. Condens. Matter 3 (1991) 8195–8204.

[19] M.F. Ruiz-Lopez, A. Munoz-Paez, A theoretical study of the XANES spectra of rutile and anatase, J. Phys. Condens. Matter 3 (1991) 8981–8990.

[20] F. Farges, G.E. Brown, J.J. Rehr, Coordination chemistry of Ti (IV) in silicate glasses and melts: I. XAFS study of titanium coordination in oxide model compounds, Geochim. Cosmochim. Acta 16 (1996) 3023–3038.

[21] Z.Y. Wu, G. Ouvrard, P. Gressier, C.R. Natoli, Ti and O K-edges for titanium oxides by multiple scattering calculations: comparison to XAS and EELS spectra, Phys. Rev. B 55 (1997) 10382–10391.

[22] D. Cabaret, Y. Joly, H. Renevier, C.R. Natoli, Pre-edge structure analysis of Ti K-edge polarized X-ray absorption spectra in TiO_2 by full-potential XANES calculations, J. Synchrotron Radiat. 6 (1999) 258–260.

[23] W.F. David, X-ray band spectra and molecular-orbital structure of rutile TiO_2, Phys. Rev. B 5 (1972) 4219–4226.

[24] A. Bianconi, E. Fritsch, G. Calas, J. Petiau, X-ray absorption near-edge structure of *3d* transition elements in tetrahedral coordination: the effect of bond-length variation, Phys. Rev. B 32 (1985) 4292–4295.

[25] F. Farges, G.E. Brown, J.J. Rehr Jr., Ti K-edge XANES studies of Ti coordination and disorder in oxide compounds: comparison between theory and experiment, Phys. Rev. B 56 (1997) 1809–1819.

[26] H. Modrow, S. Bucher, J.J. Rehr, A.L. Ankudinov, Calculation and interpretation of K-shell X-ray absorption near-edge structure of transition metal oxides, Phys. Rev. B 67 (2003) 035123.

[27] J. Chaboy, N. Nakajima, Y. Tezuka, Ab initio X-ray absorption near-edge structure study of Ti K-edge in rutile, J. Phys. Condens. Matter 19 (2007) 266206.

[28] F.M.F de Groot, Novel techniques and approaches to unravel the nature of X-ray absorption spectra, AIP Conf. Proc. 882 (2007) 37–43.

[29] X.C. Yang, M. Dubiel, D. Ehrt, A. Schütz, X-ray absorption near edge structure analysis of valence state and coordination geometry of Ti ions in borosilicate glasses, J. Non-Cryst. Solids 354 (2008) 1172–1174.

[30] A. Ramos, M. Gandais, J. Petiau, Study of nucleation process in (Li_2O, Al_2O_3, $4SiO_2$) glasses, by X-ray absorption spectroscopy and transmission electron microscopy, J. Phys. Colloq. C 8 (1985) 491–494.

[31] A. Ramos, M. Gandais, Earliest stages of crystal growth in a silicate glass containing titanium and zirconium as nucleating elements-HRTM and XAS study, J. Cryst. Growth 100 (1990) 471–480.

[32] F. Farges, G.E. Brown, J.J. Rehr, Coordination chemistry of Ti (IV) in silicate glasses and melts: II. Glasses at ambient temperature and pressure, Geochim. Cosmochim. Acta 16 (1996) 3039–3053.

[33] M. Emili, L. Incoccia, S. Mobilio, G. Fagherazzi, M. Guglielmi, Structural investigations of TiO_2–SiO_2 glassy and glass–ceramic materials prepared by the sol–gel method, J. Non-Cryst. Solids 74 (1985) 129–146.

[34] L. Cormier, P.H. Gaskell, G. Calas, A.K. Soper, Medium-range order around titanium in a silicate glass studied by neutron diffraction with isotopic substitution, Phys. Rev. B 58 (1998) 11322–11330.
[35] F. Farges, A Ti K-edge EXAFS study of the medium range environment around Ti in oxide glasses, J. Non-Cryst. Solids 244 (1999) 25–33.
[36] M. Altarelli, D.L. Dexter, H.M. Nussenzveig, Superconvergence and sum rules for the optical constants, Phys. Rev. B 6 (1972) 4502–4509.
[37] V. Maier, R. Frahm, X-ray absorption studies of the short-range order in lithium aluminosilicate glass–ceramics, Glasstech. Ber. 62 (1989) 20–28.
[38] J. Xu, C. Lind, A.P. Wilkinson, S. Pattanaik, X-ray diffraction and X-ray absorption spectroscopy studies of sol–gel-processed zirconium titanates, Chem. Mater. 12 (2000) 3347–3355.
[39] L. Galoisy, E. Pélegrin', M.A. Arrio, P. Ildefonse, G. Calas, Evidence for 6-coordinated zirconium in inactive nuclear waste glasses, J. Am. Ceram. Soc. 82 (1999) 2219–2224.
[40] T. Dumas, J. Petiau, Structural organization around nucleating elements (Ti, Zr) and Zn during crystalline nucleation process in silico-aluminate glasses, in: K.O. Hodgson, B. Hedman, J.E. Penner-Hahn (Eds.), EXAFS and Near Edge Structure III, Springer, Berlin, 1984, pp. 311–313.
[41] M.W. Barsoum, Fundamental of Ceramics, McGraw-Hill, Boston, New York, 1997, pp. 391–434.
[42] K.H. Lee, D.A. Hirschfeld, J.J. Brown, In situ reinforced glass–ceramic in the lithia–alumina–silica system, in: C. Michael, Weinberg (Eds.), Nucleation and Crystallization in Glasses and Liquids, The American Ceramic Society, Westerville, OH, 1992, pp. 293–301.